

Article

Construction Method for a Three-Dimensional Tunnel General Monomer Model Based on Parallel Pathfinding

Jiaming Ye, Defu Che, Baodong Ma *, Quan Liu, Kehan Qiu and Xiangxiang Shang

Institute for Geoinformatics & Digital Mine Research, Northeastern University, Shenyang 110819, China; 2000986@stu.neu.edu.cn (J.Y.); chedefu@mail.neu.edu.cn (D.C.); 2000977@stu.neu.edu.cn (Q.L.); 2000980@stu.neu.edu.cn (K.Q.); 2100964@stu.neu.edu.cn (X.S.)

* Correspondence: mabaodong@mail.neu.edu.cn

Abstract: Existing approaches for the 3D modeling of tunnels suffer from several problems, such as highly difficult data acquisition, redundancy of model data, large computational burden, and the inability of the resulting models to be monolithic. Therefore, solutions to the tunnel network modeling problem for complex structures need to be proposed and elaborated in detail. In this paper, a construction method for a three-dimensional tunnel general monomer model based on parallel pathfinding is proposed. Widely used tunnel CAD drawings are analyzed and read, a disordered arc ensemble intersection trend decision method is developed, and an automatic path extraction solution algorithm for unidirectional modeling of tunnel centerlines is constructed. By constructing and splicing the surface elements of the 3D model, a monomeric 3D tunnel model representing the complex network structure is finally obtained. Moreover, the modeling of shafts is realized based on the monomer model, allowing for the three-dimensional topological relationships between different sub-levels of the tunnel and the ground to be established. The automatic modeling method proposed in this paper is applied to the digital twin platform of a filling project in a mining area in Gansu province, China. The experimental results demonstrate that the 3D tunnel models constructed in this way have a smaller data volume, higher modeling accuracy, and more stable growth of modeling speed.

Keywords: tunnel; parallel; pathfinding; monomer; 3D modeling



Citation: Ye, J.; Che, D.; Ma, B.; Liu, Q.; Qiu, K.; Shang, X. Construction Method for a Three-Dimensional Tunnel General Monomer Model Based on Parallel Pathfinding. *ISPRS Int. J. Geo-Inf.* **2023**, *12*, 270. <https://doi.org/10.3390/ijgi12070270>

Academic Editors: Sisi Zlatanova and Wolfgang Kainz

Received: 16 March 2023

Revised: 14 May 2023

Accepted: 24 May 2023

Published: 6 July 2023



Copyright: © 2023 by the authors. Licensee MDPI, Basel, Switzerland. This article is an open access article distributed under the terms and conditions of the Creative Commons Attribution (CC BY) license (<https://creativecommons.org/licenses/by/4.0/>).

1. Introduction

In recent years, geographic information technology has come to play an increasingly significant role in mine construction and mining [1]. Concepts relating to digital mines and intelligent mines have been proposed [2,3], and the technologies and methods for mine data acquisition, application, and mine information technology platform construction have become richer [4]. Tunnels are an important part of underground mining. Traditional 2D tunnel data cannot accurately and intuitively describe the spatial distribution of a tunnel. Therefore, three-dimensional underground tunnel modeling technology has gradually become a popular field of research [5]. Three-dimensional tunnel models allowing for the determination of intuitive topological relationships provide data support for underground shortest path searches [6], and they can help to realize the analysis and calculation of the optimal underground disaster avoidance path through virtual simulation technology [7], establish tunnel virtual environments for mine safety management decision-making systems [8], and realize personnel positioning and personnel error analysis and research [9]. Based on a three-dimensional tunnel model, remote real-time maintenance platforms in underground mines can be established [10], and early disaster warnings based on simulation of the effect of underground environmental changes can also be realized [11].

Three-dimensional modeling techniques have been developed over many years, and numerous excellent 3D platforms such as ArcGIS Engine [12], CATIA V5 [13], Unity 3D [14] and AutoCAD have gradually been launched. However, the applicability and efficiency of

these platforms for tunnel modeling are poor. Therefore, in order to meet the development needs of mine construction, it is necessary to develop more efficient and rapid 3D monomer modeling techniques for tunnels, which can considerably reduce the complexity and difficulty of 3D model construction [15].

At present, 3D modeling methods for tunnels can be divided into three categories. Methods in the first category are conventional; these tunnel modeling methods rely on manual manipulation. Engineers need to first complete the drawing of 2D sketches, and then transfer them to professional modeling workers for 3D model construction. For example, tunnel modeling can be realized manually by using Revit software [16]. Methods in the second category fully obtain detailed spatial information of the tunnel through the use of measurement technology, such as constructing point clouds of the tunnel based on three-dimensional laser scanning [17,18], three-dimensional lidar [19,20], close-range photogrammetry technology [21], manual measurements, or other methods [22]. Further, a 3D model of the tunnel can be constructed using aerial triangulation, the Delaunay growth algorithm, or the shortest diagonalization method [23]. Methods in the third category calculate the spatial characteristics of 3D models through known parameters. For example, parametric modeling, the ArcGIS Engine [24], BIM, GIS [25], HOOPS [26], and/or other technologies can be used to achieve accurate expression of tunnel section parameters through 3D models [27]. At the same time, it is necessary to calculate and analyze the spatial topological relationships between the existing data, such as analyzing the tunnel traverse measurement data with respect to the idea of a bidirectional diagram, in order to realize three-dimensional modeling of the tunnel in terms of its components [28]. The intersection point modeling algorithm based on Boolean operation can also solve the intersection point connectivity problem and improve the accuracy of 3D modeling [29].

Among the above, the first category of modeling methods can establish detailed roadway characteristics as required, but manual intervention is required to assist in the generation of 3D models, resulting in low modeling efficiency, high labor cost, low modeling accuracy, and unstable accuracy. This complex processing process poses great obstacles in terms of productivity and cannot be applied to largescale tunnel modeling [30]. In the second category of methods, tunnel modeling methods based on laser point cloud data, photogrammetry data, and other technologies can accurately express the spatial geometry of the tunnel, but the cost of the measurement equipment is high, the data redundancy of the constructed model is high, the number of triangular mesh sheets forming the surface of the model is large, the data processing and calculation burdens are heavy, and the costs associated with storage, rendering, transmission, and other resources are high. In addition, there may be some blind spots and distortions in the measured structures, as well as some errors when the point clouds are concatenated during the construction of the model. With the maturity of internet technology, 3D modeling platforms have gradually developed from desktop to Web and mobile [31–33]. It is expected that online 3D tunnel model operation platforms will be a key development trend in the future. Therefore, it is necessary to establish three-dimensional tunnel models with smaller data volumes than the model results of the second category of methods to meet the requirements of online rendering and transmission. The third category of methods can control the amount of data modeled well, but such methods still need to be improved. For example, the modeling method based on bidirectional graphs is unable to comprehensively analyze the spatial topology of a tunnel, and the point-by-point sequential traversal modeling method is less efficient. Moreover, the resulting 3D model of the tunnel obtained by the third category of methods is always an overall 3D model that can only be viewed, which has certain limitations and fails to realize the model monomers; that is, each subsection of the tunnel cannot be directly used to complete independent management, attribute querying, attribute addition, and other functions. Most of the correlation algorithms in this category of methods currently used for 3D tunnel modeling focus on the modeling of simple tunnel structures and cannot be applied effectively to the construction of 3D tunnel models possessing complex network structures. Additionally, little research has been conducted on the application of models

using online platforms, and the convenience of dynamic updating and rendering of non-monomeric tunnel models in online platforms is poor. Many modeling approaches do not implement vertical axis modeling and cannot establish topological relationships between different segments.

Therefore, based on the existing problems of the above methods, this paper proposes a construction method for a three-dimensional tunnel general monomer model based on parallel pathfinding. Combined with the tunnel distribution information and tunnel section structure data stored in the two-dimensional traverse measurement data widely used in mines, the automatic and rapid construction of a tunnel model can be realized through parallel routing modeling, improving the modeling speed. Compared with traditional CAD software, it realizes the automation of spatial information extraction and three-dimensional model construction of tunnels and avoids complex interactive operations. The resulting model can accurately express information about the spatial topology of tunnels, the structure of the tunnels, and the splicing of tunnels at intersections. The accuracy of the three-dimensional model can reduce the data redundancy and calculation burden, thus meeting the requirements for practical application in the mining field, and the sub-segments of the tunnel model can be flexibly and independently managed in the form of monomeric units. The proposed model can effectively solve the problems of insufficient modeling efficiency, limited model function, and difficulties in updating online when considering complex tunnel networks.

2. Materials and Methods

The modeling program proposed in this paper is based on the OpenSceneGraph (OSG) 3D engine and was developed using the C++ programming language. The CAD data and tunnel section data widely used in mines were used as data sources. According to the coordinate information of a disordered arc set in the CAD drawings, the automatic detection and calculation of tunnel topological relations in complex scenes, such as single, two-pass, multi-pass, loop, and network topologies, can be realized. In the proposed method, the complex network arc set is organized and sorted, and the modeling path is extracted, the centerline topology relationships are reconstructed, the network topology structure of the whole disordered point and line set is obtained, and the monomer 3D model of each tunnel subsegment is constructed by extending along the path direction. In this way, the problem of fast automatic modeling from the tunnel centerline network of a complex tunnel is solved, and a fast and accurate modeling process from 2D tunnel CAD drawing data to a 3D model of the complex tunnel network can be carried out. Based on analysis of the characteristics of two-dimensional section data of the tunnel, an inversion method between two-dimensional sections and three-dimensional models of the underground tunnel is effectively established by analyzing the geometric and topological characteristics of the tunnel model, according to the real spatial attributes of the tunnel shape, arch height, and wall height in the field, in order to achieve a full and equal proportion corresponding between the tunnel section in the three-dimensional scene and the design of the two-dimensional tunnel section. Furthermore, the proposed approach can be customized, according to the application needs, to establish tunnel models of varying precision. The technical route of automated 3D tunnel modeling is shown in Figure 1.

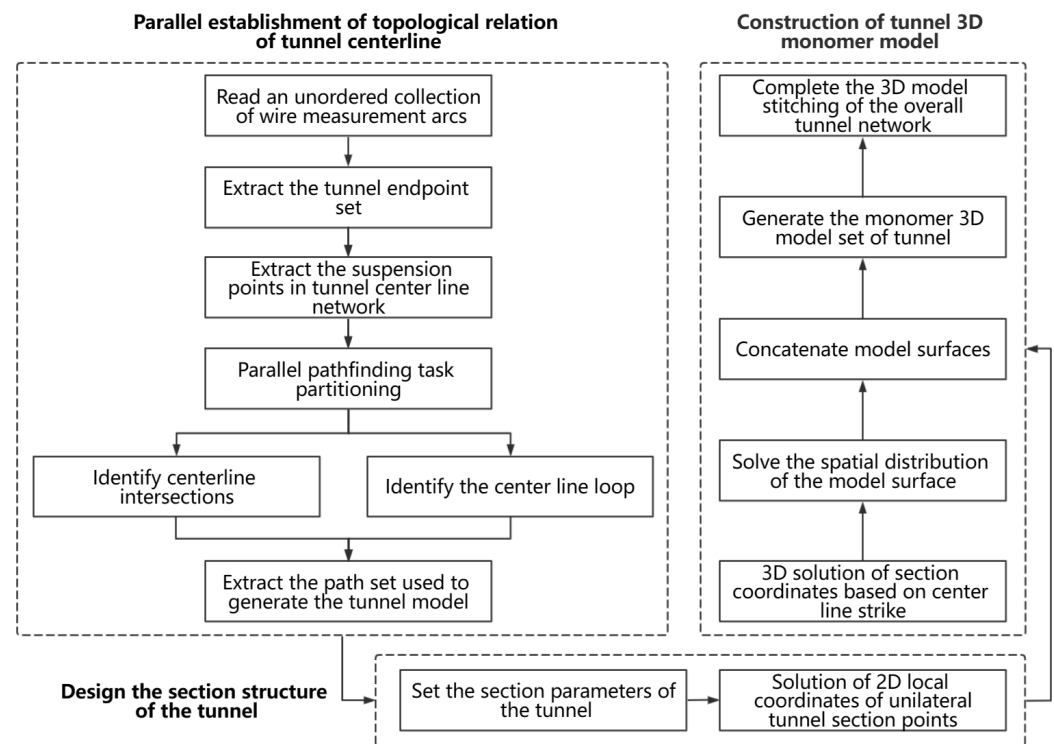


Figure 1. Technical route of automated 3D tunnel modeling.

2.1. Construction of Automatic Topological Relations for the Centerline of the Tunnel

2.1.1. Calculating the Direction of the Tunnel Crossing

At present, the most widely used form of tunnel data in practical mining applications is 2D CAD drawing data, with the DXF file format as the general CAD data exchange format. In this paper, the open source C++ library DXFLib is used to process the DXF files of the tunnels and to solve the problem of parsing and reading the CAD tunnel data. The construction of the topological relationships in the tunnel model relies on the set of directed paths formed by all nodes of the tunnel along the directions of the different branches. Thus, it is necessary to establish topological relationships for the disordered set of arcs corresponding to the centerlines of tunnels in the original data. Due to the complex structure of the tunnel network, a pathfinding modeling method based on the centerline of the tunnel is proposed, which gradually partitions the complex network into a set of independent unidirectional modeled centerline paths. When the model construction is completed on both sides of all centerlines, the complete modeling and stitching of the entire complex tunnel network can be achieved.

The measurement plane rectangular coordinate system, rather than the mathematical plane rectangular coordinate system, is used for tunnel drawings commonly used in mines. The difference between the two coordinate systems is shown in Figure 2, where Figure 2a shows the mathematical coordinate system and Figure 2b shows the measuring coordinate system. The measuring coordinate system and the mathematical coordinate system are different in three aspects:

(1) The axes are differently oriented: the mathematical coordinate system has the X-axis as the horizontal axis and the Y-axis as the vertical axis, while the measurement coordinate system has the Y-axis as the horizontal axis and the X-axis as the vertical axis.

(2) Quadrants I, II, III, and IV in the mathematical coordinate system are arranged in the counterclockwise direction, while the four quadrants of the measurement coordinate system are arranged in the clockwise direction.

(3) The azimuth angle of the mathematical coordinate system starts from 0° in the positive direction of the X-axis and increases in the counterclockwise direction, with the value ranging from 0° to 360° , while the azimuth angle α of the measurement coordinate

system starts from 0° in the positive direction of the X-axis and the magnitude of the azimuth increases in the clockwise direction, ranging from 0° to 360° .

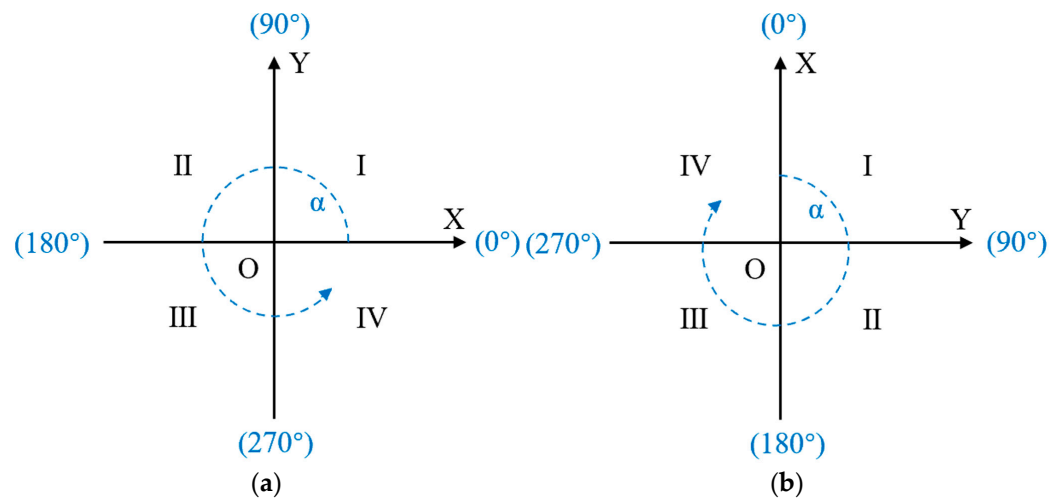


Figure 2. Mathematical coordinate system and measuring coordinate system: (a) mathematical coordinate system with quadrants arranged counterclockwise; (b) measuring coordinate system with quadrants arranged clockwise.

As the structure of underground tunnels is often complex and staggered, there are typically a large number of intersections in the tunnel network, including different forms (e.g., three-way and multi-way) forming a large number of branches with different directions. In the unidirectional modeling of pathfinding along the centerline, it is necessary to compute the direction of the crossing points to ensure consistent turning during automatic pathfinding, thus avoiding modeling routes being missed and duplicate modeling. Tunnel pathfinding modeling at intersections is depicted in Figure 3. The directions of branches connected by intersections may be distributed in four quadrants in the metric frame. Turning rules need to be established for automated modeling, with a unified decision method covering all intersections.

For the ordinary inflection point shown in Figure 3a, the nodes at P_1 and P_2 create a point vector $\vec{P_1P_2}$ along the centerline on the left side of the unidirectional model, and the modeling path directly extends to P_3 . When the intersection point is the intersection of complex branches, the modeling path starts from point P_1 to point P_2 . For the remaining node vectors from P_2 (i.e., $\vec{P_2P_3}$, $\vec{P_2P_4}$, $\vec{P_2P_5}$, $\vec{P_2P_6}$, and $\vec{P_2P_7}$), the coordinate azimuth values (i.e., α_{23} , α_{24} , α_{25} , α_{26} , and α_{27} , respectively) in the azimuth set A are calculated. At the same time, the coordinate azimuth α_{21} of the opposite vector $\vec{P_2P_1}$ of vector $\vec{P_1P_2}$ is included into the azimuth set A, and the azimuth values in A are sorted. The ordering of the azimuth angle α_{21} in A can result in three cases, as shown in Figure 3b–d. Figure 3b shows the situation where the azimuth angle α_{21} is maximal in A. In this case, P_3 should be selected as the next unidirectional modeling node to ensure the correct construction of the unidirectional model of the tunnel; that is, α_{23} has the smallest azimuth angle and should be selected, such that the corresponding vector $\vec{P_2P_3}$ is the extension direction of the modeling path. Figure 3c shows the case where the azimuth angle α_{21} is minimal in A. In this case, the vector $\vec{P_2P_3}$, whose azimuth angle is just larger than α_{21} , should be taken as the extension direction of the modeling path. Figure 3d shows the case where the magnitude order of azimuth α_{21} is neither maximal nor minimal in A. In this case, the orientation $\vec{P_2P_6}$ should be the modeling extension direction, as the azimuth angle α_{26} of this vector is just larger than α_{21} .

Therefore, the modeling path extension decision method can be further simplified into two cases: in the azimuth set A, when the azimuth α_{21} of the opposite vector in the starting

direction is maximal, the direction of the minimum azimuth is taken as the modeling direction; and, when the azimuth α_{21} of the opposite vector of the starting direction is not maximal, the direction whose azimuth is the next-largest when compared to α_{21} is taken as the modeling direction.

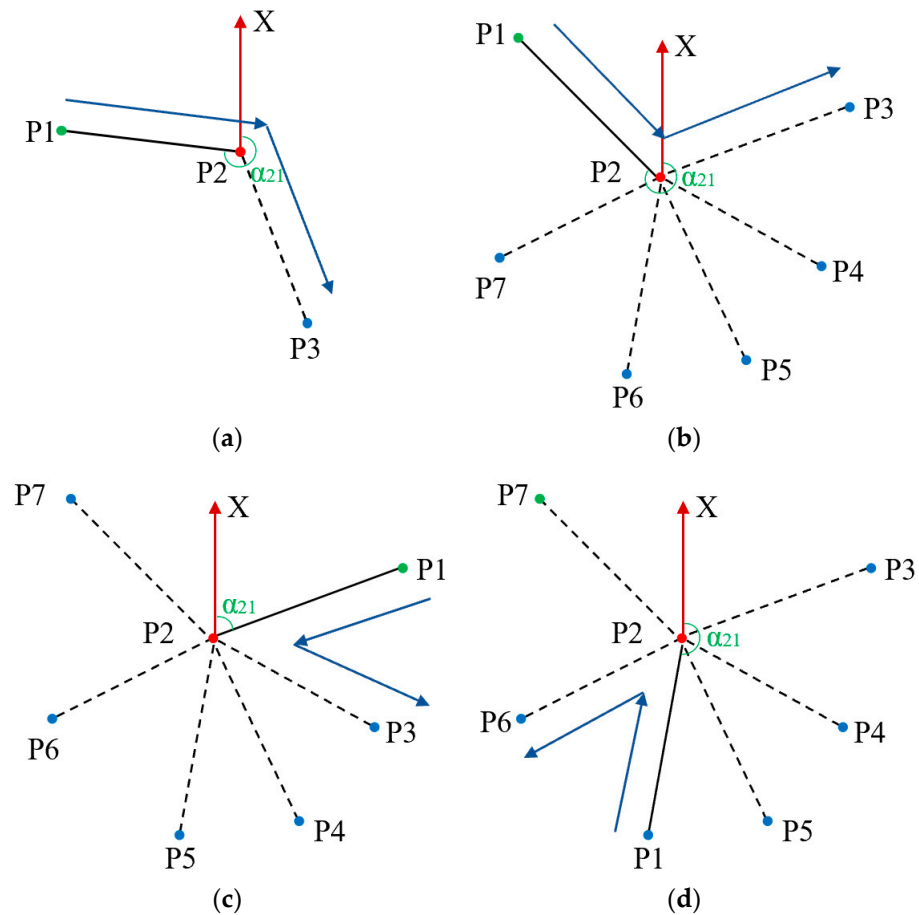


Figure 3. The direction judgment for tunnel intersection pathfinding: (a) ordinary inflection point; (b) azimuth α_{21} is the largest; (c) azimuth α_{21} is the smallest; (d) azimuth α_{21} is neither the largest nor smallest.

2.1.2. Path Extraction Strategy for Parallel Modeling

A thread is the basic unit of CPU scheduling and allocation, used to execute a specific instruction in a program. Using multi-threading techniques, a set of time segments can be created for executing instructions. In a multicore processor environment, these time segments can be juxtaposed on multiple cores, and multiple instructions can be run simultaneously in parallel time segments, thus realizing parallel execution by multi-threading. For computational tasks with high complexity, if the tasks can be clearly separated into several independent tasks based on their characteristics, then multi-threading methods can be used to efficiently utilize idle CPU time segments and improve the efficiency of the algorithm.

In the process of pathfinding, the modeling method proposed in this paper only reads and does not modify the tunnel centerline and node data. All of the sub-paths for modeling are unique, and the storage of each modeling path after extraction does not affect the unmodeled path. Moreover, the crossover trend judgment method described above is applicable to any of the intersection points in a tunnel network. Therefore, multiple starting points can be established for the modeling pathfinding task, the repetitive complex operations can be effectively organized, and multiple modeling paths can be independently established in parallel and synchronously by using a crossover trend determination method,

allowing for a large number of modeling paths to be quickly extracted. Figure 4 shows a flowchart of the parallel tunnel pathfinding provided by the proposed modeling algorithm.

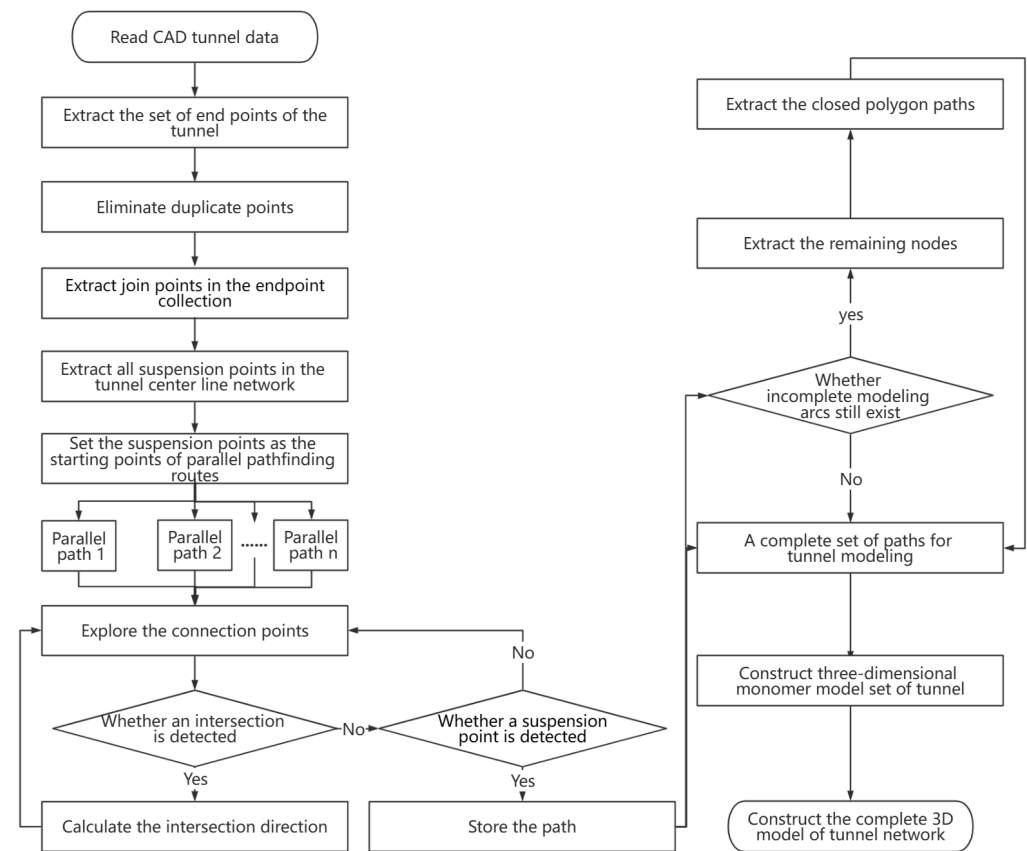


Figure 4. Flow chart of pathfinding tunnel modeling method.

The specific steps are as follows:

(1) Read the set of tunnel arcs. The DXFLib open source library is used to read the DXF format tunnel drawing files, obtain the layer where the tunnel centerline is located in the drawings, and obtain the tunnel arc set G_L required for modeling. For the curve paths existing in the tunnel network, multiple fitting line segments formed by the curves are obtained by means of fitting point extraction and are also stored in the arc segment set G_L .

(2) Extraction of tunnel node set. The starting and ending points of all arcs are obtained by traversal, and all overlapping points are eliminated to obtain the node set G_p for the tunnel network.

(3) Extract all suspension points. In the tunnel node set, nodes connected with only one other node are called suspension points. All suspension points are stored in the set G_s , as shown in Figure 5a.

(4) Multi-threaded parallel task grouping. The efficiency of multi-threaded operations depends on the number of multi-core CPU processors. The algorithm in this paper is designed for CPU-intensive applications with multi-threading. If the number of CPU processors in the current computer is m , the number of parallel tasks n is set to $m + 1$, according to the characteristics of CPU-intensive applications. If the number of suspension points in the tunnel network is less than n , the number of tasks is consistent with the number of suspension points; if the number of suspension points in the tunnel network is greater than n , the tasks are grouped into groups of size n .

(5) Parallel extraction path modeling. Each suspension point in each group obtained in step (4) is set as a starting point, and parallel path exploration is conducted in a multi-threaded manner, that is, finding the modeling path to the next point connected to each starting point. When the path extends to a crossing point, the next point of the path is

decided according to the tunnel crossing point calculation method described above. When each path extends to another suspension point, then an independent modeling path is found, and the latter suspension point is the endpoint of this modeling path, as shown in Figure 5b–e. Repeat this step to complete modeling path extraction for all suspension points in each group. There can be loops and non-loops in the tunnel network, among which there may be intra-loop branches with suspension points, for which this method is also applicable.

(6) Summarize incomplete modeling arcs. When all suspension points in the tunnel network have been submitted to modeling path extraction, check whether there are unidirectional and bidirectional unmodeled arcs in the navigation tunnel network; for example, there may be unidirectional unmodeled arcs inside a completely closed loop in the tunnel or bidirectional unmodeled arcs on the common side of two loops.

(7) Path extraction for closed loop modeling. The unidirectional and bidirectional unmodeled arcs obtained in step (5) form several closed polygons in the tunnel network, and all independent closed polygons are extracted by using the left-turn algorithm directly [34]. The directed modeling path for each closed tunnel is formed by ordering the vertices of each polygon clockwise, as shown in Figure 5d.

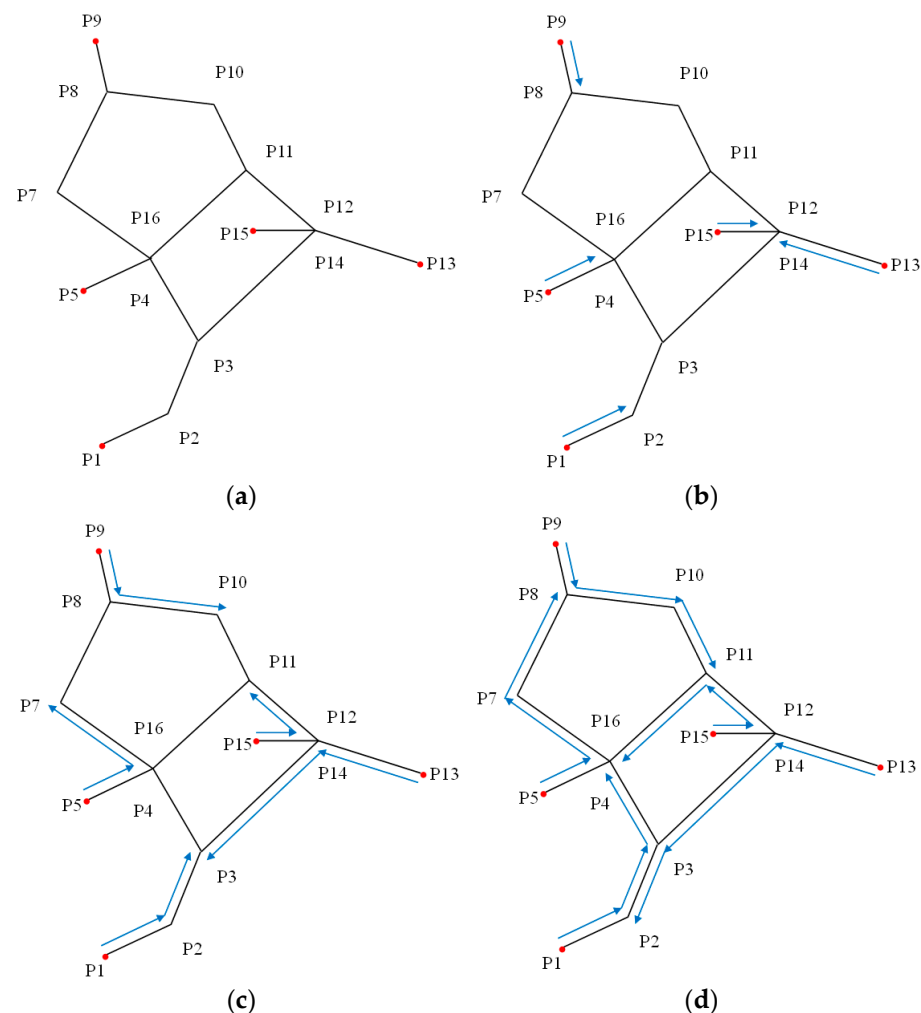


Figure 5. Cont.

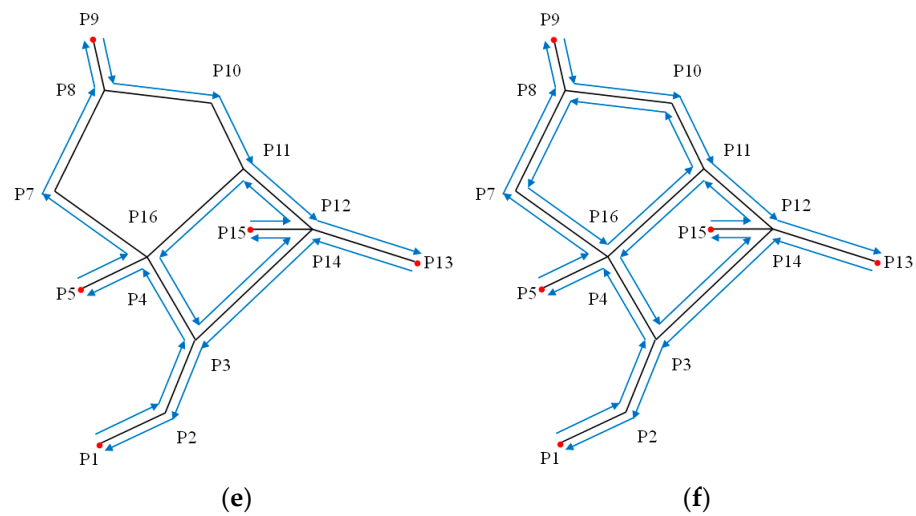


Figure 5. Extraction of tunnel unidirectional modeling paths: (a) extract suspension points, which are marked by red points in the figure; (b) parallel pathfinding begins, with paths marked by blue lines; (c) parallel pathfinding process; (d) parallel pathfinding process; (e) complete path extraction with suspension points; (f) complete closed path extraction.

2.2. Setting of Tunnel Section Parameters

A tunnel section refers to a cross-section perpendicular to the centerline of a tunnel. Due to differences in lithology, ground pressure, and mining technology, the types of tunnel section structure adopted in mining also differ. Tunnel sections can be divided into trapezoidal, rectangular, polygon, semicircular arch, circular arch, and three-centered arch sections, among others. Taking a circular arch as an example, this paper analyzes the distribution of a tunnel section in a two-dimensional local coordinate system. The circular arch takes a part of a certain circle to form the tunnel arch. The arch is smooth and consistent, and it is not easy to produce a stress concentration under the action of pressure around the tunnel, providing the supporting structure with a good stress state. This type of profile has a high utilization rate, can reduce the required amount of excavation work, and has a simple construction technique. See Figure 6 for a schematic view of a circular arch tunnel section.

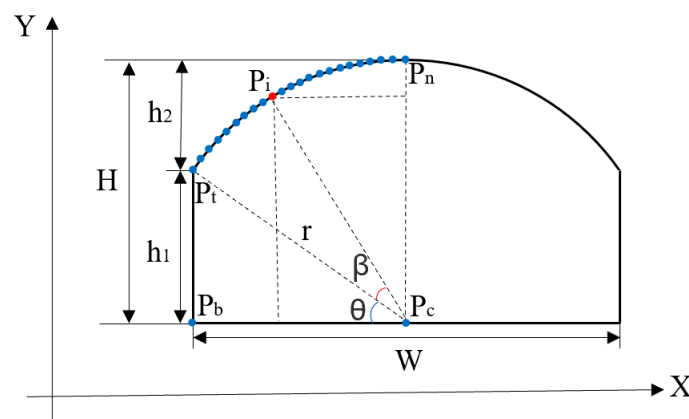


Figure 6. Cross-sectional view of a circular arch tunnel.

In Figure 6, h_1 is the wall height, h_2 is the arch height, H is the total height of the tunnel, W is the width of the tunnel, r is the radius corresponding to the top of the arc, P_c is the known centerline coordinate (corresponding to a node of the tunnel centerline network in the CAD drawing), P_b is the bottom point of the left wall of the tunnel, P_t is the top point of the left wall of the tunnel, and P_n is the vault point of the tunnel. The radian value of $\angle P_b P_c P_t$ is expressed as θ , and the radian value of $\angle P_t P_c P_i$ is expressed as β . P_i

refers to each point on the arc top of the tunnel, which is usually formed by multi-line segment fitting in computer graphics, where i refers to the number of arc points in a single arch of the tunnel section. The larger the value of i , the higher the precision, which can be set according to the actual rendering requirements. In order to ensure that the 3D tunnel model is consistent with the real tunnel section structure, the tunnel width W , wall height h_1 and arch height h_2 of the tunnel section are set according to the actual tunnel section. The calculation formulas for each tunnel section point are as follows:

$$\begin{cases} x_{Pb} = x_{Pc} - \frac{W}{2} \\ y_{Pb} = y_{Pc} \end{cases}, \quad (1)$$

$$\begin{cases} x_{Pt} = x_{Pc} - \frac{W}{2} \\ y_{Pt} = y_{Pc} + h_1 \end{cases}, \quad (2)$$

$$\begin{cases} x_{Pn} = x_{Pc} \\ y_{Pn} = y_{Pc} + h_1 + h_2 \end{cases}, \quad (3)$$

$$\begin{cases} \theta = \arctan \frac{2h_1}{W} \\ \beta = d\alpha \times i \end{cases}, \quad (4)$$

$$\begin{cases} x_{Pi} = x_{Pc} - r \times \cos(\theta + \beta) \\ y_{Pi} = y_{Pc} + r \times \sin(\theta + \beta) \end{cases}. \quad (5)$$

In the formulas above, the coordinates of each parameter are the coordinates in the corresponding two-dimensional local coordinate system of the section, where x_{Pc} , y_{Pc} , x_{Pb} , y_{Pb} , x_{Pt} , y_{Pt} , x_{Pi} , y_{Pi} , x_{Pn} , and y_{Pn} are the X and Y coordinates of P_c , P_b , P_t , P_i , and P_n , respectively.

2.3. Monomeric Three-Dimensional Tunnel Model Construction Method

By using the calculation method for the tunnel section parameters described above and the path extraction algorithm for tunnel network modeling, the coordinate positions of tunnel sections in the two-dimensional local coordinate system and the coordinates of tunnel center points contained in the obtained paths can be obtained. Moreover, the points P_c in the tunnel cross-section diagram are the central points of the tunnel, corresponding to the nodes in the modeling path. Therefore, the conversion from two-dimensional section points of the tunnels to three-dimensional spatial coordinates can be realized.

As shown in Figure 7a,b, point P_2 is the inflection point on the path. The offset path of paths P_1P_2 and P_2P_3 is used to calculate the intersection point P_2' , following which the unidirectional unit vector \vec{v}_2 corresponding to point P_2 can be obtained according to the coordinates of the tunnel center point and the unit vector \vec{v}_2 . With respect to the nodes in the tunnel modeled path from P_1 to P_2 , we obtain the tunnel unit vector \vec{v}_{12} in the horizontal direction and the vertical unit vector \vec{v}_1 . As shown in Figure 7c, according to the tunnel section point calculation method, the coordinate offset values dx and dy for each tunnel section point relative to the known central point P_c in the two-dimensional local coordinate system can be obtained. The vector \vec{v}_1 in Figure 7a–c is the same vector. The unit vector \vec{v}_1 is used to calculate the three-dimensional coordinates of the roadway points on the left side of the centerline. According to the spatial characteristics of the tunnel, the tunnel section is perpendicular to the horizontal direction, the positive direction of the Y-axis in the two-dimensional local coordinate system corresponds to the positive direction of the vertical Z-axis in the three-dimensional coordinate system, and the negative direction of the X-axis in the two-dimensional local coordinate system corresponds to the direction

of the unit vector \vec{v}_1 . The calculation method for the three-dimensional coordinates of the suspension point of the initial centerline is as follows:

$$\vec{P}_{txy} = \vec{P}_{cxy} + |dx| \times \vec{v}_1 \tag{6}$$

$$P_{tz} = P_{cz} + h_1 \tag{7}$$

where \vec{P}_{cxy} denotes the x- and y-coordinates of the tunnel center point P_c represented by a vector in the three-dimensional coordinate system; \vec{P}_{txy} denotes the x-coordinates and y-coordinates of the tunnel point P_t , represented by a vector in the three-dimensional coordinate system; P_{cz} denotes the z-coordinate of the tunnel center point in the three-dimensional coordinate system; and P_{tz} denotes the z-coordinate of the tunnel point P_t in the three-dimensional coordinate system. Formulas (6) and (7) may also be used to calculate the three-dimensional coordinates of the set of tunnel section points corresponding to the turning point P_2 .

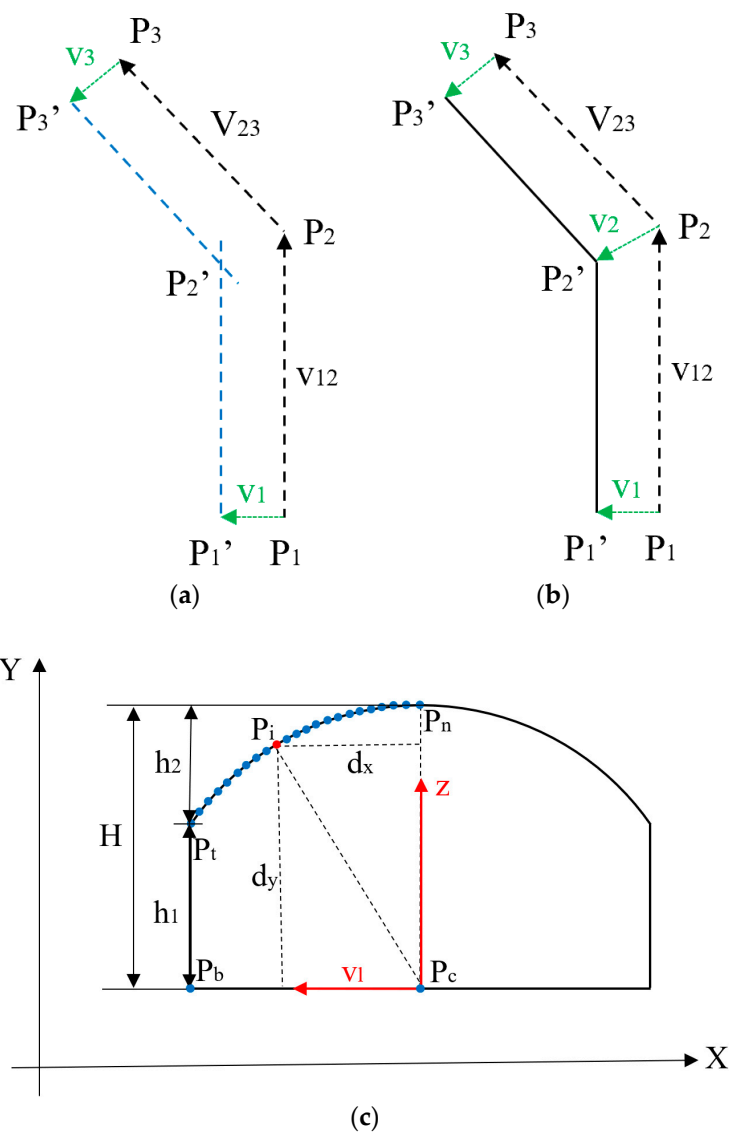


Figure 7. Diagram of the process of solving 3D coordinates: (a) obtain the intersection point of the tunnel boundary lines; (b) obtain the offset vector corresponding to the inflection point; (c) calculate the offset values of each section point in the tunnel 2D local coordinate system.

Through the above methods of path extraction and coordinate solution, the three-dimensional coordinates of the bidirectional point sets for all sections in the tunnel network can be obtained. As shown in Figure 8a, taking the six sections A, B, C, D, E, and F shown in the figure as examples, the surface elements ABED and BCFE are formed by connecting the corresponding points of the sections of adjacent nodes. Surface elements are obtained according to this method, then spliced to build the model surface, as shown in Figure 8b. In the modeling process, an accurate connection is established between the starting and ending center points of each arc segment in the coordinate sets of the corresponding tunnel section points. The starting and ending points of the centerline are used to match the two unidirectional tunnels corresponding to each arc segment, and the monomer model of the tunnel corresponding to each centerline arc segment is established. The monomer tunnel is independently stored and derived as an independent obj model. At the same time, the basic attribute values of tunnel and vertex values for each face are exported in the form of a JSON file. In the JSON file, the ID of each monomeric tunnel segment corresponds to the name of a unique obj file. As the ancillary data used in this modeling method, JSON files have good universality and practicality. Taking the data types in the C++ programming language used in this article as an example, the basic attributes of the monomer models are shown in Table 1.

Table 1. Basic properties of monomer tunnel model.

Attribute	Data Type	Data Format
ID	int	i
Coordinates of the starting point	vector<float>	(x_s, y_s, z_s)
Coordinates of the end point	vector<float>	(x_e, y_e, z_e)
Coordinate set of cross-section points on the left side of the starting point	vector<vector<float>>	$(x_{s1}, y_{s1}, z_{s1}), (x_{s2}, y_{s2}, z_{s2}), (x_{s3}, y_{s3}, z_{s3}), \dots$
Coordinate set of cross-section points on the right side of the starting point	vector<vector<float>>	$(x_{s1}', y_{s1}', z_{s1}'), (x_{s2}', y_{s2}', z_{s2}'), (x_{s3}', y_{s3}', z_{s3}'), \dots$
Coordinate set of cross-section points to the left of the end point	vector<vector<float>>	$(x_{e1}, y_{e1}, z_{e1}), (x_{e2}, y_{e2}, z_{e2}), (x_{e3}, y_{e3}, z_{e3}), \dots$
Coordinate set of cross-section points on the right side of the end point	vector<vector<float>>	$(x_{e1}', y_{e1}', z_{e1}'), (x_{e2}', y_{e2}', z_{e2}'), (x_{e3}', y_{e3}', z_{e3}'), \dots$
The face vertex coordinate set of the model on the left	vector<vector<vector<float>>>	$[(x_{l11}, y_{l11}, z_{l11}), (x_{l12}, y_{l12}, z_{l12}), (x_{l13}, y_{l13}, z_{l13}), (x_{l14}, y_{l14}, z_{l14})], [(x_{l21}, y_{l21}, z_{l21}), (x_{l22}, y_{l22}, z_{l22}), (x_{l23}, y_{l23}, z_{l23}), (x_{l24}, y_{l24}, z_{l24})], [(x_{l31}, y_{l31}, z_{l31}), (x_{l32}, y_{l32}, z_{l32}), (x_{l33}, y_{l33}, z_{l33}), (x_{l34}, y_{l34}, z_{l34})], \dots$
The face vertex coordinate set of the model on the right	vector<vector<vector<float>>>	$[(x_{r11}, y_{r11}, z_{r11}), (x_{r12}, y_{r12}, z_{r12}), (x_{r13}, y_{r13}, z_{r13}), (x_{r14}, y_{r14}, z_{r14})], [(x_{r21}, y_{r21}, z_{r21}), (x_{r22}, y_{r22}, z_{r22}), (x_{r23}, y_{r23}, z_{r23}), (x_{r24}, y_{r24}, z_{r24})], [(x_{r31}, y_{r31}, z_{r31}), (x_{r32}, y_{r32}, z_{r32}), (x_{r33}, y_{r33}, z_{r33}), (x_{r34}, y_{r34}, z_{r34})], \dots$

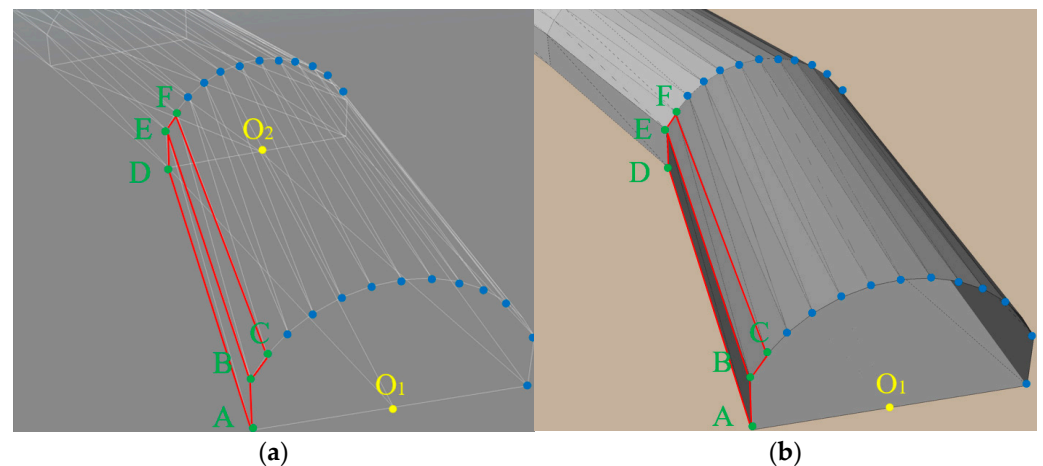


Figure 8. Construction of tunnel model: (a) connect the corresponding section points, which are marked by blue points in the figure; (b) construct the surface elements of the model.

2.4. Shaft Modeling Methods Based on Monomeric Models

In mining areas, shafts are used to establish connections between the ground and different sub-levels of the tunnel. Therefore, when modeling tunnels, it is necessary to implement shaft modeling to establish complete spatial topological relationships between different sub-level tunnel networks. A shaft in a tunnel can mainly be in a straight tunnel section, inflection point, or multi-pass position, as shown in Figure 9.

In the cases where the shaft is located in a straight tunnel, the shaft is projected on the plane where the bottom of the tunnel is located, where the center of the projection circle of the shaft is perpendicular to the direction of the tunnel centerline, and the monomer subsegment of the tunnel is divided into two monomer models, as shown in Figure 9a. When the shaft is located in a straight or multi-passage tunnel, the tunnel is divided by the angle bisector formed by the centerline of the tunnel, as shown in Figure 9b,c. In order to achieve the connectivity effect, the joint reconstruction of the arches and shafts at the top of the tunnel is a key problem in axial modeling. First, the connectivity of the shaft at the inflection point of a tunnel is discussed. The modeling method is as follows:

(1) Projection of dividing shaft. In the XOY horizontal plane, the projection of the axis in the horizontal plane is divided into four regions (A, B, C, and D), according to the intersection line and the centerline of the two tunnel sub-sections.

(2) Obtain the intersection line. Taking area a as an example, Figure 10a shows the schematic diagram of a tunnel vault and floor, while Figure 10b shows the schematic diagram of the intersection of a shaft and tunnel vault. The projection of the starting and ending points onto the XOY plane is obtained by using the section points of the starting and ending points in the monomer model. The horizontal plane projection of the connecting line CC_1 —which is closest to the center of the circle and the radius R of the shaft section—is taken as the tangent line, and the XOY plane coordinates of the intersection point $D_2 \sim I_2$ of the connecting line between the arch section and the shaft projection are obtained. The actual Z-coordinates corresponding to the vault points $D_2 \sim I_2$ can be obtained using the elevation interpolation of the starting point and the ending point of the monomer unidirectional tunnel. In Equation (8), Z_P is the Z-coordinate of the intersection point, Z_S is the Z-coordinate of the starting point of the connection line, Z_E is the Z-coordinate of the end point of the connection line, D_{SP} is the distance from the starting point of the connection line to the intersection point in the horizontal plane, and D_{SE} is the distance from the starting point of the connection line to the end point of the connection line in the horizontal plane:

$$Z_P = Z_S + (Z_E - Z_S) \times \frac{D_{SP}}{D_{SE}} \quad (8)$$

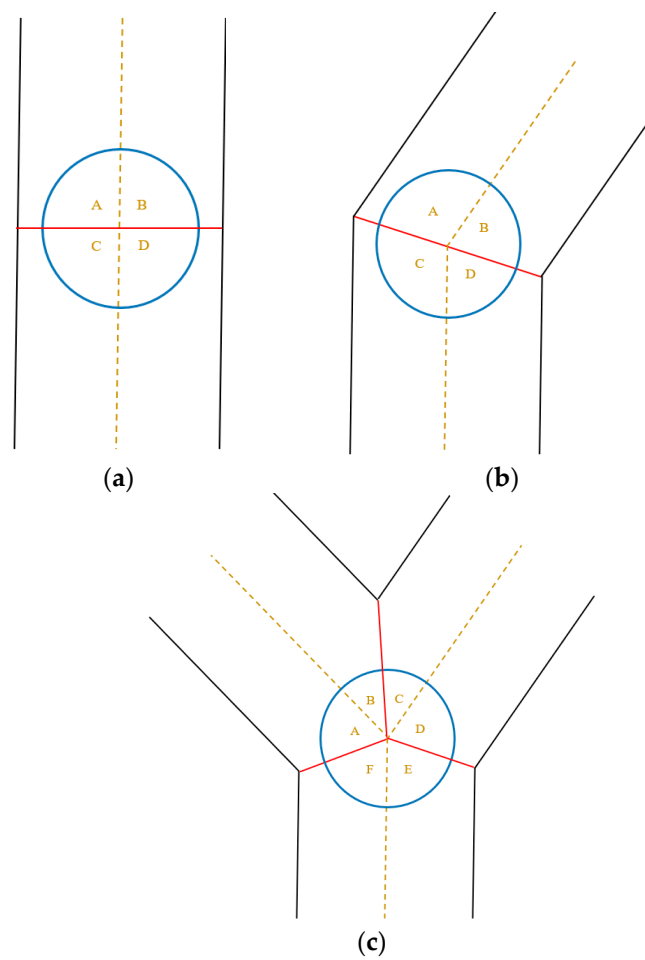


Figure 9. The relative relationship between a shaft and a tunnel: (a) the shaft projection is divided into four regions on the straight tunnel (A, B, C, and D); (b) the shaft projection is divided into four regions on the turning point of tunnel (A, B, C, and D); (c) the shaft projection is divided into six regions on the tunnel intersection (A, B, C, D, E and F).

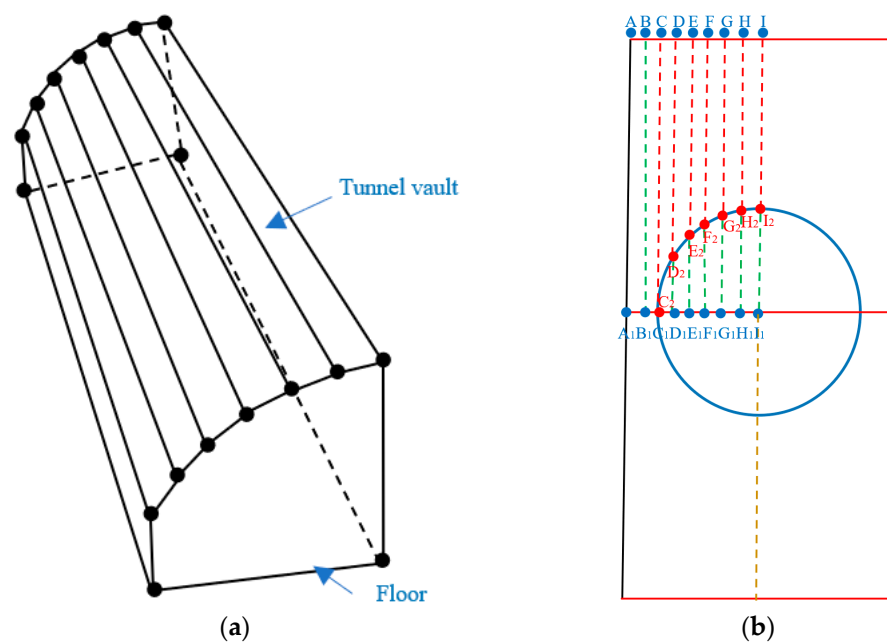


Figure 10. Cont.

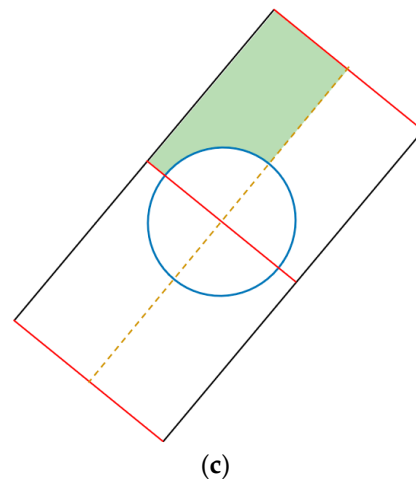


Figure 10. The joint of the vault and floor of a tunnel with a shaft: (a) tunnel vault and floor; (b) the intersection of a shaft and a tunnel vault, where the dotted line is the line of the corresponding points of the section, the red dotted line indicates that the line of the corresponding points of the section intersects the shaft projection; (c) the intersection of a shaft and the floor of a tunnel, the green area is the new area after the floor or ground is divided.

(3) Coordinate calculation of intersection points at the bottom of the shaft. The three-dimensional coordinates of the points $C_2 \sim I_2$ obtained in step (2) are used to obtain the intersection points for regions b, c, and d. The intersection points of the four regions are arranged in sequence, and the curve intersection lines between the shaft and the top surface of the tunnel are constructed by means of multi-segment line fitting. The points of the multi-segment lines are the bottom edge points of the shaft.

(4) Coordinate calculation of intersection points at the top of the shaft. Each point of the intersection line obtained in step (3) is extended vertically upward to the plane where the upper tunnel floor is located, in order to obtain the intersection line point at the top of the shaft.

(5) Shaft modeling. Vertical shaft modeling can be realized by using the top and bottom edge points obtained in steps (3) and (4), as well as the method of surface construction based on the adjacent points and corresponding points (as shown in Figure 8). The vertical shaft modeling accuracy is consistent with the set tunnel vault modeling accuracy.

(6) Reconstruction of lower tunnel vault model. The corresponding points A_1 and B_1 of the connection lines tangential to and intersecting with the circle are retained, and the original tunnel section points $C_1 \sim I_1$ are replaced by the points $C_2 \sim I_2$. The tunnel is reconstructed using the face construction method shown in Figure 8 to realize the hollow unidirectional tunnel vault. In other areas, the lower tunnel vault model is reconstructed according to steps (2)–(4).

(7) Model reconstruction of upper tunnel floor (or ground). The upper tunnel floor is a simple structure with polygonal planes. The method of region separation detailed in step (1) is still adopted to obtain the top edge point of the shaft in this area, extending to the upper tunnel floor in step (4). By replacing the vertex of the unidirectional tunnel floor in the original area covered by this group of section points, floor reconstruction in this area can be realized, as shown in Figure 10c. The reconstruction of the remaining areas of the floor of the tunnel (or ground) in the model is also completed according to the abovementioned steps, in order to realize reconstruction of the upper floor of the tunnel. The ground reconstruction method is carried out similarly.

The above method is applicable in the case where the shaft is located in a straight or multi-passage tunnel. However, the case of the turning point of a tunnel requires a special discussion. As shown in Figure 11a, if the corresponding angle θ is obtuse after the vertical shaft projection is separated by a unidirectional tunnel, the unidirectional tunnel sub-segment should be further divided into left and right sections by using the vertical

line OH in the direction of the connection line between the center of the circle O and the corresponding point of the tunnel section, as shown in Figure 11b. The two sections may also adopt the modeling idea mentioned above, in order to complete the shaft modeling and splicing.

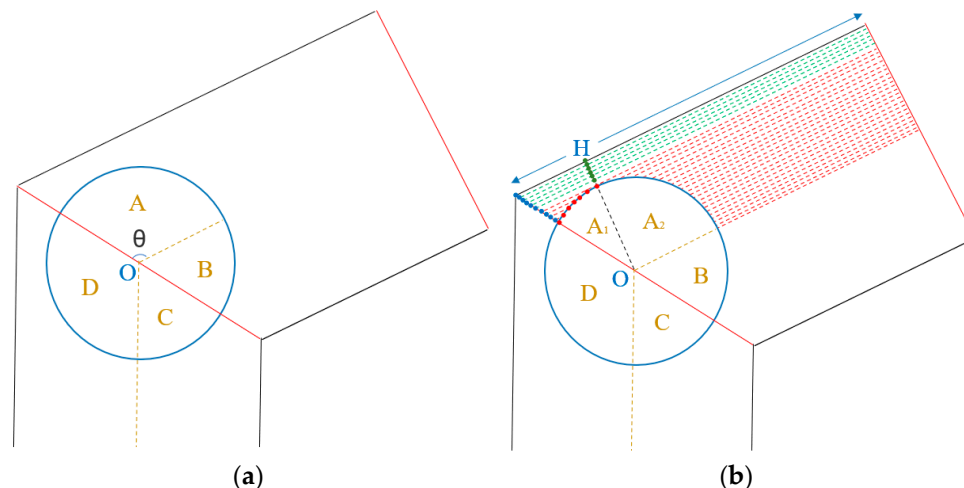


Figure 11. The intersection of the turning point of a tunnel and a shaft: (a) angle of turning point of tunnel; (b) the intersection area is further segmented, region A is divided into two parts, A_1 and A_2 .

3. Results and Analysis

To verify the effectiveness of this method, in this paper, a 12th generation Intel(R) Core(TM) i9-12900H 2.50GHz CPU, NVIDIA RTX A2000 8GB GPU, 64GB RAM, Windows 11 \times 64 operating system was used for experiments.

Taking the underground tunnel of a metal mine in Gansu Province, China as an example, 3D tunnel network models consisting of different sub-levels were established, which were applied to the underground tunnel module of an intelligent filling digital twin platform, providing functions such as platform filling pipeline topology analysis, underground disaster virtual simulation, filling simulation, and downhole equipment parameter analysis and calculation. Figure 12 shows the interface used for setting tunnel model section parameters.

Figure 13 shows the comparison between the effect of the 3D model with 1050 sub-levels for the mining area and that of the CAD data. After many experiments, it was found that the general monomeric model construction method for 3D tunnels based on parallel automated pathfinding proposed in this paper could effectively read all of the data of the centerline layer for the target tunnel in the CAD data, realizing rapid automatic model establishment. The structure of the 3D tunnel model was consistent with the real data, and the modeling accuracy was always stable. The modeling speed was linearly positively correlated with the number of node points and inflection points in the tunnel network. The spatial accuracy and practicality of the data were much better than those when using the original tunnel CAD drawings. Therefore, the proposed method can meet the network data high-speed transmission and information development-related practical application requirements in the mining field.

In this paper, the modeling speed of the proposed modeling method was tested, and the three-dimensional modeling of a tunnel with different numbers of nodes was carried out. We used tunnels with different numbers of nodes and compared the proposed method with two existing tunnel modeling methods, as shown in Table 2. Among the quantitative test results for different tunnels, the speed of the modeling method proposed in this paper was superior to the other two methods, and the results show that the time required for tunnel modeling increased linearly with the increase in tunnel nodes.

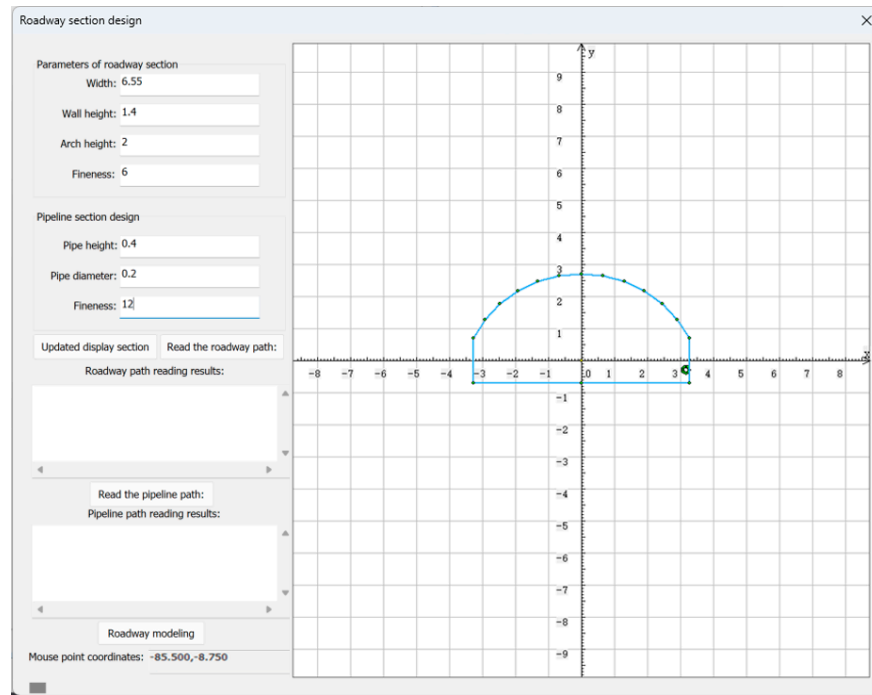


Figure 12. Parameter setting for tunnel section, and tunnel sections are marked with blue lines.

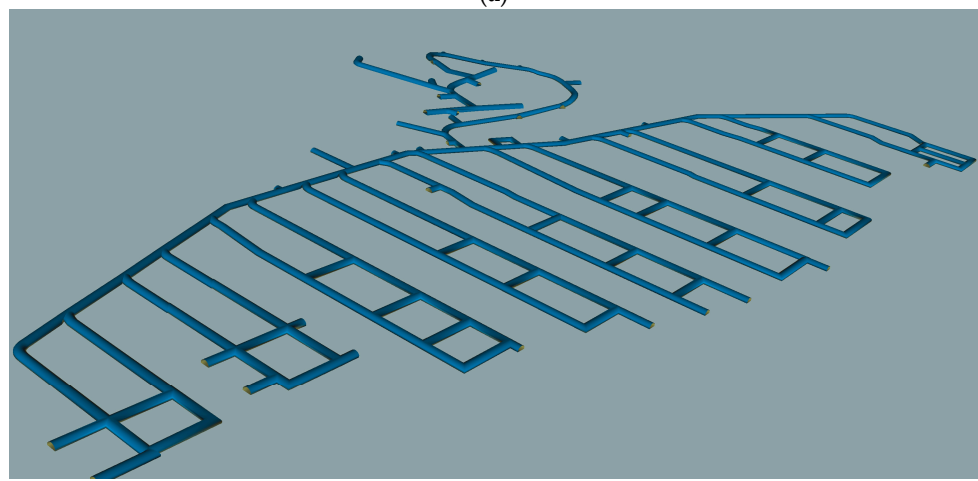
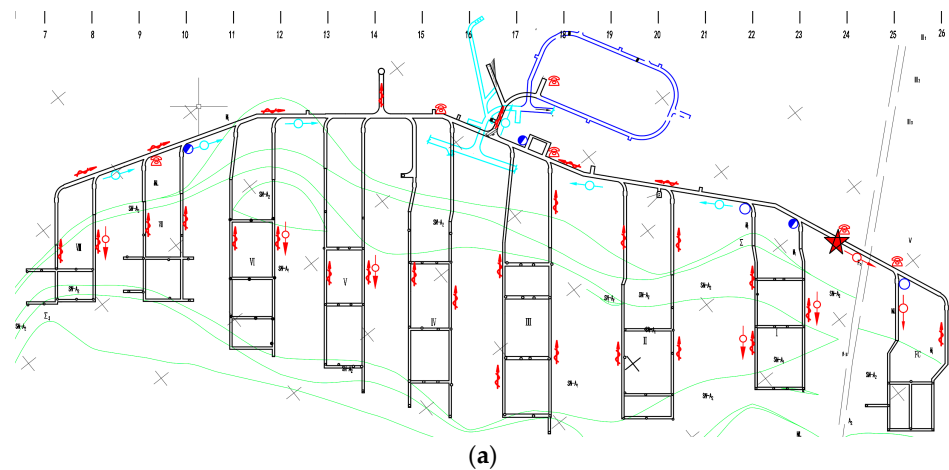


Figure 13. Comparison of CAD drawing and 3D model of tunnels: (a) CAD drawings of tunnels; (b) the result of tunnel modeling.

Table 2. Comparison of modeling speeds of different methods.

Method	The Number of Nodes in the Tunnel Network	Modeling Time (ms)
Automatic 3D entity modeling method for landway system based on measure wire data	565	3268
	1298	8653
	3532	20,359
	5684	35,997
Component-based 3D modeling method for complex mine tunnel network	565	1061
	1298	2698
	3532	6077
	5684	11,890
Construction method for a three-dimensional tunnel general monomer model based on parallel pathfinding	565	783
	1298	1683
	3532	4051
	5684	7918

Figure 14a,b show monomer models of tunnel sub-segments. The monomer models corresponding to the independent obj models are characterized by universality and can be directly loaded and rendered on different platforms. The monomer models can facilitate the functions of flexible interactive operation, additional attributes, and independent modification in practical applications. The monomeric tunnel modeling method can realize independent management and independent attribute assignment of tunnel subsegments. When some tunnel subsegments are filled or disasters occur, the monomeric tunnel subsegment model can achieve independent highlighting, management and operation of the target subsegments without complicated model clipping and other calculations. When the mining area of a local tunnel area changes, only the specified subsegment can be modified, without modifying the entire tunnel network model. In the online three-dimensional mine platform, the modified tunnel subsegment monomer model needs to be transmitted and updated after the local tunnel changes, which greatly reduces the efficiency of network transmission and updating.

The attribute values in the JSON file can be obtained using any platform developed using a programming language that supports JSON interpretation, allowing for the monomeric tunnel models with basic attributes to be easily obtained. At the same time, the JSON files contain vertex information of the faces in the monomeric tunnel model. In other platforms, this vertex information can be used to directly generate a complete model. In online platform applications, the obj model can also be directly replaced by JSON files as the transmitted data. Figure 14c shows the independent interactive operation of a monomer model in a digital twin platform developed using the C# programming language and based on the Unity platform.

Figure 15a shows the effect of shaft modeling, while Figure 15b shows the application of the shaft model in a digital twin platform. The shaft is closely connected with the tunnel, thus meeting the requirements for practical application. The shaft connects different sub-segments of a tunnel and provides data support for filling process simulation of filling digital twin platforms.

Figure 16 shows the overall tunnel network modeling effect and its application in the digital twin platform. In practical application, the tunnel model realizes the intuitive expression of the spatial characteristics of underground mining. In this paper, file sizes after modeling of different sections of tunnel were tested, and the results are shown in Table 3. The results show that, compared with the second type of method mentioned in the introduction, the tunnel model generated by the method proposed in this paper greatly reduces the storage space requirements for the file. The size of each monomer tunnel model file is less than 10KB, which provides an advantage in the online transmission and rendering process for the digital twin platform.

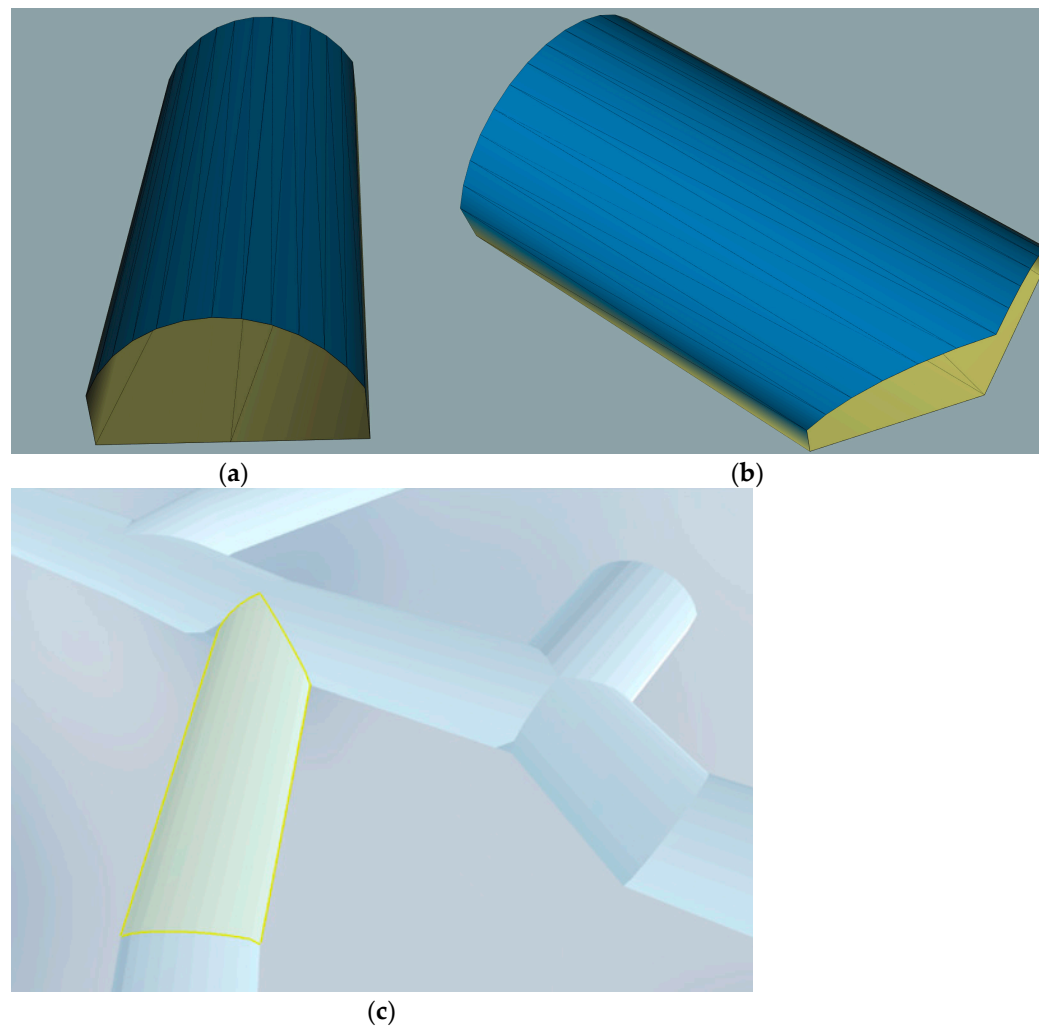


Figure 14. Tunnel sub-segment monomer modeling: (a) monomeric tunnel model; (b) monomeric tunnel model; and (c) interactive operation of the monomeric tunnel model.



Figure 15. Shaft 3D modeling: (a) the effect of shaft modeling; and (b) application of shaft model in a digital twin platform.

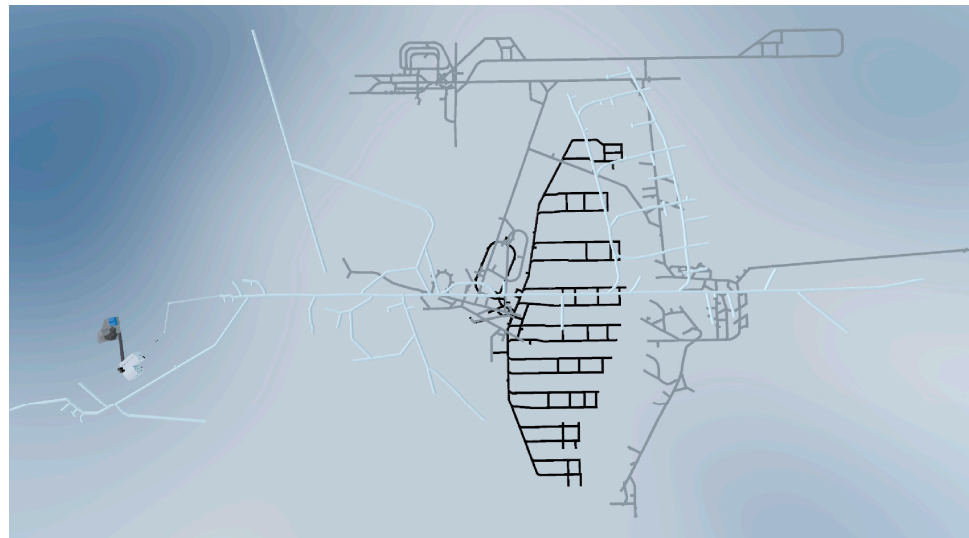


Figure 16. Application of 3D tunnel network model in a digital twin platform.

Table 3. The size of each sub-segment roadway model file.

Number of Sub-Segments	Number of Tunnel Arcs	Size of Model File (KB)
1050	3685	17,948
1150	7739	53,942
1350	2537	30,996

The idea of the modeling algorithm proposed in this paper can be applied to the three-dimensional model construction of tunnels having any section shape. By further extending the algorithm, the three-dimensional geometry of linear ground objects with any section shape can be rapidly modeled in an automated manner using this method. For example, it can be effectively applied to the design and modeling of walls, ditches, roads, pipeline networks, etc. Figure 17 shows an example of the application of the three-dimensional tunnel modeling method proposed in this paper to the design of ditches in a 3D governance design platform for a real scene in a mining area.

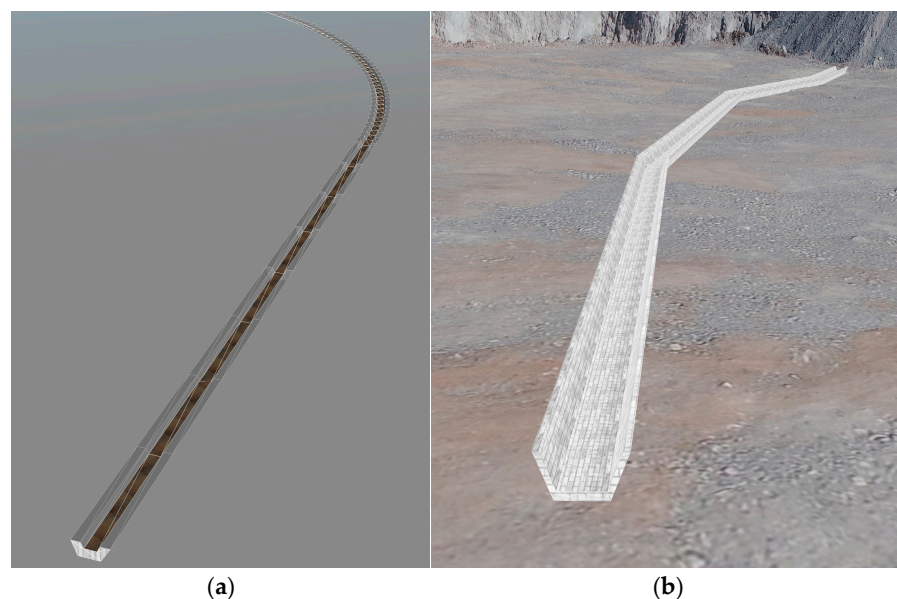


Figure 17. Application examples of channel modeling: (a) the effect of channel modeling; and (b) rendering of ditch modeling in a practical application.

4. Conclusions

In order to solve the problems associated with high modeling difficulty and data redundancy when conducting complex tunnel network modeling, we proposed a construction method for three-dimensional tunnel general monomer models based on parallel automated routing that can effectively utilize existing CAD tunnel drawing data. Moreover, the CAD data can be analytically processed to construct a 3D tunnel model that accurately reflects the spatial distribution and topological relational structure of the complex tunnel network. The main conclusions of this study are as follows:

(1) Analyzing and classifying all actual tunnel intersections in an underground tunnel, in order to elaborate the modeling path extraction method based on a disordered tunnel arc segment set, allows for complex situations such as common inflection points, complex intersection points, closed loops, and inner loop branches to be effectively solved, thus realizing automated tunnel modeling path extraction.

(2) A construction method for a monomeric three-dimensional tunnel model was proposed, in order to realize the independent management of sub-segments in a tunnel network. The organization method of JSON, as auxiliary data for modeling, was also discussed. The proposed monomeric model is universal and can play a relevant role in different platforms, particularly in realizing the block transmission of tunnel models to online platforms.

(3) On the basis of the tunnel monomer model, shaft modeling was realized. The connection between the shaft and subsections of straight tunnels, the intersection of tunnels, and the turning point of tunnels were discussed. The coordinates of shaft section points were calculated using the idea of projection area segmentation, which allows for the close splicing of shaft and tunnel models, and the connection relationships between different tunnel sub-levels and shafts were established.

The 3D tunnel modeling method proposed in this paper was tested and applied in a digital twin platform for a mining area in Gansu Province, China. It realized the automatic and rapid modeling of a multi-section complex tunnel network with high modeling accuracy, good stitching effect, small space occupancy of the model data, strong modeling performance, and stable growth of the modeling speed with the complexity of the tunnel network. The monomeric roadway model enhances the function of independent management for model sub-segments. The automatic pathfinding modeling method proposed in this paper can be further expanded and effectively applied to model construction scenes such as roads, ditches, walls, pipe networks, etc., in order to achieve three-dimensional modeling of linear ground objects having any section shape.

Author Contributions: Conceptualization, Jiaming Ye and Baodong Ma; Data curation, Defu Che, Baodong Ma, Quan Liu, Kehan Qiu and Xiangxiang Shang; Formal analysis, Defu Che, Baodong Ma and Kehan Qiu; Funding acquisition, Baodong Ma; Investigation, Quan Liu and Xiangxiang Shang; Methodology, Jiaming Ye; Project administration, Defu Che; Resources, Baodong Ma and Xiangxiang Shang; Software, Jiaming Ye; Supervision, Defu Che and Kehan Qiu; Validation, Defu Che; Visualization, Jiaming Ye and Kehan Qiu; Writing—original draft, Jiaming Ye. All authors have read and agreed to the published version of the manuscript.

Funding: This research was conducted with support from the National Natural Science Foundation of China (41871310) and the Fundamental Research Funds for the Central Universities (N2124005, N2001020).

Data Availability Statement: The data presented in this study are available from the corresponding author upon reasonable re-quest.

Conflicts of Interest: The authors declare no conflict of interest.

References

1. Nag, R.; O'Rourke, S.M.; Cummins, E. A GIS study to rank Irish agricultural lands with background and anthropogenic concentrations of metal(loid)s in soil. *Chemosphere* **2022**, *286*, 131928. [[CrossRef](#)]
2. Wang, L.H. From Intelligence Science to Intelligent Manufacturing. *Engineering* **2019**, *5*, 615–618. [[CrossRef](#)]

3. Zhang, K.X.; Kang, L.; Chen, X.X.; He, M.C. A Review of Intelligent Unmanned Mining Current Situation and Development Trend. *Energies* **2022**, *15*, 513. [[CrossRef](#)]
4. Zhang, Z.Z.; Bai, J.B.; Chen, Y.; Yan, S. An innovative approach for gob-side entry retaining in highly gassy fully-mechanized longwall top-coal caving. *Int. J. Rock Mech. Min. Sci.* **2015**, *80*, 1–11. [[CrossRef](#)]
5. Li, W.J.; Li, S.Y.; Lin, Z.Y.; Li, Q. Information modeling of mine working based on BIM technology. *Tunn. Undergr. Space Technol.* **2021**, *115*, 103978. [[CrossRef](#)]
6. Wang, F.; Shi, L.; Fan, W.; Wang, C. Application of computational geometry in coal mine tunnel 3D localization. *Int. Arab J. Inf. Technol.* **2018**, *15*, 668–674.
7. Kurtz, W.; Lapin, A.; Schilling, O.S.; Tang, Q.; Schiller, E.; Braun, T.; Hunkeler, D.; Vereecken, H.; Sudicky, E.; Kropf, P.; et al. Integrating hydrological modelling, data assimilation and cloud computing for real-time management of water resources. *Environ. Modell. Softw.* **2017**, *93*, 418–435. [[CrossRef](#)]
8. Cheng, W.M.; Hu, X.M.; Xie, J.; Zhao, Y.Y. An intelligent gel designed to control the spontaneous combustion of coal: Fire prevention and extinguishing properties. *Fuel* **2017**, *210*, 826–835. [[CrossRef](#)]
9. Liu, J.; Zhang, R.; Song, D.Z.; Wang, Z.Q. Experimental investigation on occurrence of gassy coal extrusion in coalmine. *Saf. Sci.* **2019**, *113*, 362–371. [[CrossRef](#)]
10. Zhang, Y.Y.; Shao, W.; Zhang, M.J.; Li, H.J.; Yin, S.J.; Xu, Y.J. Analysis 320 coal mine accidents using structural equation modeling with unsafe conditions of the rules and regulations as exogenous variables. *Accid. Anal. Prev.* **2016**, *92*, 189–201. [[CrossRef](#)]
11. Rezaei, M.; Majdi, A.; Monjezi, M. An intelligent approach to predict unconfined compressive strength of rock surrounding access tunnels in longwall coal mining. *Neural Comput. Appl.* **2014**, *24*, 233–241. [[CrossRef](#)]
12. Li, S.; Zhou, Y.; Sun, G.X. Pipeline 3D Modeling Based on High-Definition Rendering Intelligent Calculation. *MATH PROBL ENG.* **2022**, *2022*, 1–11. [[CrossRef](#)]
13. Fabian, M.; Puškár, M.; Boslai, R.; Kopas, M.; Kender, Š.; Huňady, R. Design of experimental vehicle specified for competition Shell Eco-marathon 2017 according to principles of car body digitisation based on views in 2D using the intuitive tool Imagine & Shape CATIA V5. *Adv. Eng. Softw.* **2018**, *115*, 413–428.
14. Li, Y.X.; Zhu, Y.Y. Research on Key Technologies of Garbage Classification Virtual Simulation Game Development Based on unity3d Technology. *Procedia Comput. Sci.* **2022**, *208*, 546–552. [[CrossRef](#)]
15. Nan, L.; Bagas, L.; Li, X.H.; Xiao, K.Y.; Li, Y.; Ying, L.J.; Song, X.L. An improved buffer analysis technique for model-based 3D mineral potential mapping and its application. *Ore Geol. Rev.* **2016**, *76*, 94–107.
16. Chen, Z.; Chen, X.Q.; Liu, P.; Jia, Y.C.; Luo, C. Research on digital mine modeling based on BIM technology. *China Min. Mag.* **2022**, *31*, 73–78.
17. Shi, X.X.; Wang, J.; Wang, L.; Li, Z.Y.; Fu, H.L. Three-dimensional modelling of mine laneways under point cloud data. *Remote Sens. Inf.* **2019**, *34*, 99–104.
18. Ghabraie, B.; Ren, G.; Smith, J.; Holden, L. Application of 3D laser scanner, optical transducers and digital image processing techniques in physical modelling of mining-related strata movement. *Int. J. Rock Mech. Min.* **2015**, *80*, 219–230. [[CrossRef](#)]
19. Yi, C.; Lu, D.N.; Xie, Q.; Liu, S.Y.; Li, H.; Wei, M.Q.; Wang, J. Hierarchical tunnel modeling from 3D raw LiDAR point cloud. *Comput.-Aided Des.* **2019**, *114*, 143–154. [[CrossRef](#)]
20. Deshpande, S.S. Tunnel modeling using mobile mapping lidar points. *Int. Arch. Photogramm. Remote Sens. Spat. Inf. Sci.* **2021**, *XLIV-M-3-2021*, 23–28. [[CrossRef](#)]
21. Liu, J.; Lian, Z.Z.; He, R.; Zhang, R.R.; Zhang, H.Z. 3D modeling of underground tunnel based on close range photogrammetry technique. *Met. Min.* **2020**, *9*, 179–183.
22. Janus, J.; Ostrogórski, P. Underground Mine Tunnel Modelling Using Laser Scan Data in Relation to Manual Geometry Measurements. *Energies* **2022**, *15*, 2537. [[CrossRef](#)]
23. Chen, L.X.; Zhao, M.N. Mine Laneway Modeling and Realization Based on the Matlab. *Adv. Mater. Res.* **2013**, *690–693*, 3512–3516. [[CrossRef](#)]
24. Xie, J.L.; Zhang, D.Q. Parametric modeling and visualization of 3D mine laneway. *Min. Surv.* **2017**, *45*, 5–9.
25. Li, M.; Kang, J.T.; Liu, H.; Li, Z.Y.; Liu, X.; Zhu, Q.; Xiao, B.H. Study on parametric 3D modeling technology of mine tunnel based on BIM and GIS. *Coal Sci. Technol.* **2022**, *50*, 25–35. [[CrossRef](#)]
26. Tan, Z.H.; Pan, M.; Wang, L.G.; Tan, J.Y.; Sun, C. An automatic 3D entity modeling method for landway system based on measure wire data. *Sci. Surv. Mapp.* **2017**, *42*, 164–170.
27. Li, W.J.; Jiao, Y.H.; Qiu, L.; Zhang, X.X.; Ren, D.J. Parametric modeling of mine tunnel based on dynamo. *Met. Min.* **2022**, *555*, 63–70.
28. Jia, Q.R.; Che, D.F.; Zhong, R.Q. Component-based 3D modeling method for complex mine tunnel network. *J. Northeast. Univ.* **2020**, *41*, 1774–1780.
29. Wang, H.J.; Lu, X.M.; Li, J.L.; Zhang, S.B. Research and application of precise tunnel modeling based on boolean operation. *Softw. Guide.* **2021**, *20*, 21–25.
30. Park, J.; Kim, T.; Baek, S.Y.; Lee, K. An algorithm for estimating surface normal from its boundary curves. *J. Comput. Des. Eng.* **2015**, *2*, 67–72. [[CrossRef](#)]
31. Williams, G.; Gheisari, M.; Chen, P.J.; Irizarry, J. BIM2MAR: An Efficient BIM Translation to Mobile Augmented Reality Applications. *J. Manag. Eng.* **2015**, *31*, A4014009. [[CrossRef](#)]

32. Al Kharouf, R.A.; Alzoubaidi, A.R.; Jweihan, M. An integrated architectural framework for geoprocessing in cloud environment. *Spat. Inf. Res.* **2017**, *25*, 89–97. [[CrossRef](#)]
33. Wang, L.L. Modeling method of underground tunnel intersection processing based on binary space partition tree. *Coal Min. Saf.* **2022**, *53*, 138–143.
34. Liu, C.Z. Polygon auto-construction based on improved left-turn algorithm. *Bull. Surv. Mapp.* **2018**, *A01*, 266–268, 282.

Disclaimer/Publisher’s Note: The statements, opinions and data contained in all publications are solely those of the individual author(s) and contributor(s) and not of MDPI and/or the editor(s). MDPI and/or the editor(s) disclaim responsibility for any injury to people or property resulting from any ideas, methods, instructions or products referred to in the content.